For reprint orders, please contact:
reprints@futuremedicine.com

RESEARCH ARTICLE

Controlling the surface coverage and arrangement of proteins using particle lithography

Johnpeter N Ngunjiri, Stephanie L Daniels, Jie-Ren Li, Wilson K Serem & Jayne C Garno†

†Author for correspondence Louisiana State University and the Center for BioModular, Multi-Scale Systems, Chemistry Department, 232 Choppin Hall, Baton Rouge, LA 70803, USA Tel.: +1 225 578 8942; Fax: +1 225 578 3458; E-mail: jgarno@lsu.edu

Aims: The applicability of particle lithography with monodisperse mesospheres is tested with various proteins to control the surface coverage and dimensions of protein nanopatterns. **Methods & Materials:** The natural self-assembly of monodisperse spheres provides an efficient, high-throughput route to prepare protein nanopatterns. Mesospheres assemble spontaneously into organized crystalline layers when dried on flat substrates, which supply a structural frame or template to direct the placement of proteins. The template particles are displaced with a simple rinsing step to disclose periodic arrays of protein nanopatterns on surfaces. **Results & Discussion:** The proteins are attached securely to the surface, forming nanopatterns with a measured thickness of a single layer. The morphology and diameter of the protein nanostructures can be tailored by selecting the diameter of the mesospheres and choosing the protein concentration. **Conclusions:** Particle lithography is shown to be a practical, highly reproducible method for patterning proteins on surfaces of mica, glass and gold. High-throughput patterning was achieved with ferritin, apoferritin, bovine serum albumin and immunoglobulin-G. Depending on the ratio of proteins to mesospheres, either porous films or ring structures were produced. This approach can be applied for fundamental investigations of protein-binding interactions of biological systems in surface-bound bioassays and biosensor surfaces.

Keywords: apoferritin, atomic-force microscopy, bovine serum albumin, ferritin, immunoglobulin-G, nanopatterns, particle lithography, self-assembly

Patterning proteins is important for emerging nanoscale biological and medical applications [1,2]. There are few tools for writing or inscribing structures at the nanoscale and this problem has been approached using electron- or ion-beam lithography techniques, reactive ion-etching systems, high-powered lasers and clean rooms. Such methods are costly, require special skills, equipment or facilities and are not accessible readily to an average laboratory. There is a need for economical methods that can create reproducibly organized arrays of nanomaterials with high throughput and low cost. Particle lithography provides an approach for rapidly preparing millions of exquisitely uniform nanometer-sized structures on flat surfaces using conventional benchtop chemistry steps of mixing, centrifuging, evaporation and drying. Particle lithography, which is often referred to as nanosphere lithography, uses submicron-sized spherical particles as a mask or template to produce nanostructures on surfaces. This technique has been applied successfully to produce arrays of polymers [3–6], proteins [7–10], metals [11–19], vertical nanorods/pillars [20,21], carbon nanotubes [22] and self-assembled monolayers [23–25]. Robust, regular arrays of nanostructures can be generated reproducibly with well-defined dimensions, thickness and arrangement, even for fragile biological systems, such as proteins.

Protein patterning is a critical technology for the integration of biomolecules into miniature biological-electronic devices. Direct applications of protein patterning are found in biosensing, medical implants, control of cell adhesion and growth and for fundamental studies of cell biology [26,27]. Surface-bound arrays of protein patterns have been applied for antibody screening [28,29], testing protein activities [30] and for the analysis of antibody–antigen interactions [31]. Proteins, such as bovine serum albumin (BSA), immunoglobulin-G (IgG) and staphylococcus protein A, have been patterned with particle lithography [9,10].

Understanding the interactions of protein binding to substrates or antibodies provides essential groundwork towards developing new technologies for biosensing. Immobilized biomolecules on surfaces serve as the receptor and in some cases as the signal transducer in biosensors and biochips. Surface-bound arrays of protein nanostructures provide a test platform that is probed readily using atomic-force microscopy (AFM). Using AFM for analysis enables label-free detection of pathogens and provides a means to monitor molecular interactions in real-time under physiological solutions [32,33]. Detection for AFM is based on high-resolution imaging, as well as force and

10.2217/17435889.3.4.529 ISSN 1743-5889

height measurements and, therefore, does not require signal amplification, which can introduce error. For protein studies, the drying step can cause denaturation of a portion of the surface-bound proteins. In addition, proteins tend to aggregate and form multilayers when dried. The random, irregular distribution and surface coverage of proteins and problems with denaturation are detrimental for quantitation with surface-based assays. Therefore, the placement of biological ligands in precisely defined locations can increase the density of sensor elements and lead to improved detection limits and molecular-level control of the surface reactivity [34,35]. Miniaturization of protein arrays provides high array densities, which reduce the quantities of analytes and sample volumes required for analysis dramatically.

Materials & methods

Materials & reagents

Ferritin and apoferritin were obtained from MP Biomedical Inc. (Solon, OH, USA). BSA and rabbit IgG were purchased from Sigma Biochemicals (St Louis, MO, USA) and used without further purification. Monodisperse latex and silica spheres were acquired from Duke Scientific (Palo Alto, CA, USA). Hydrogen peroxide (30%) and sulfuric acid (95.5%) were acquired from Sigma-Aldrich (St Louis, MO, USA).

Figure 1. Particle lithography steps with proteins.

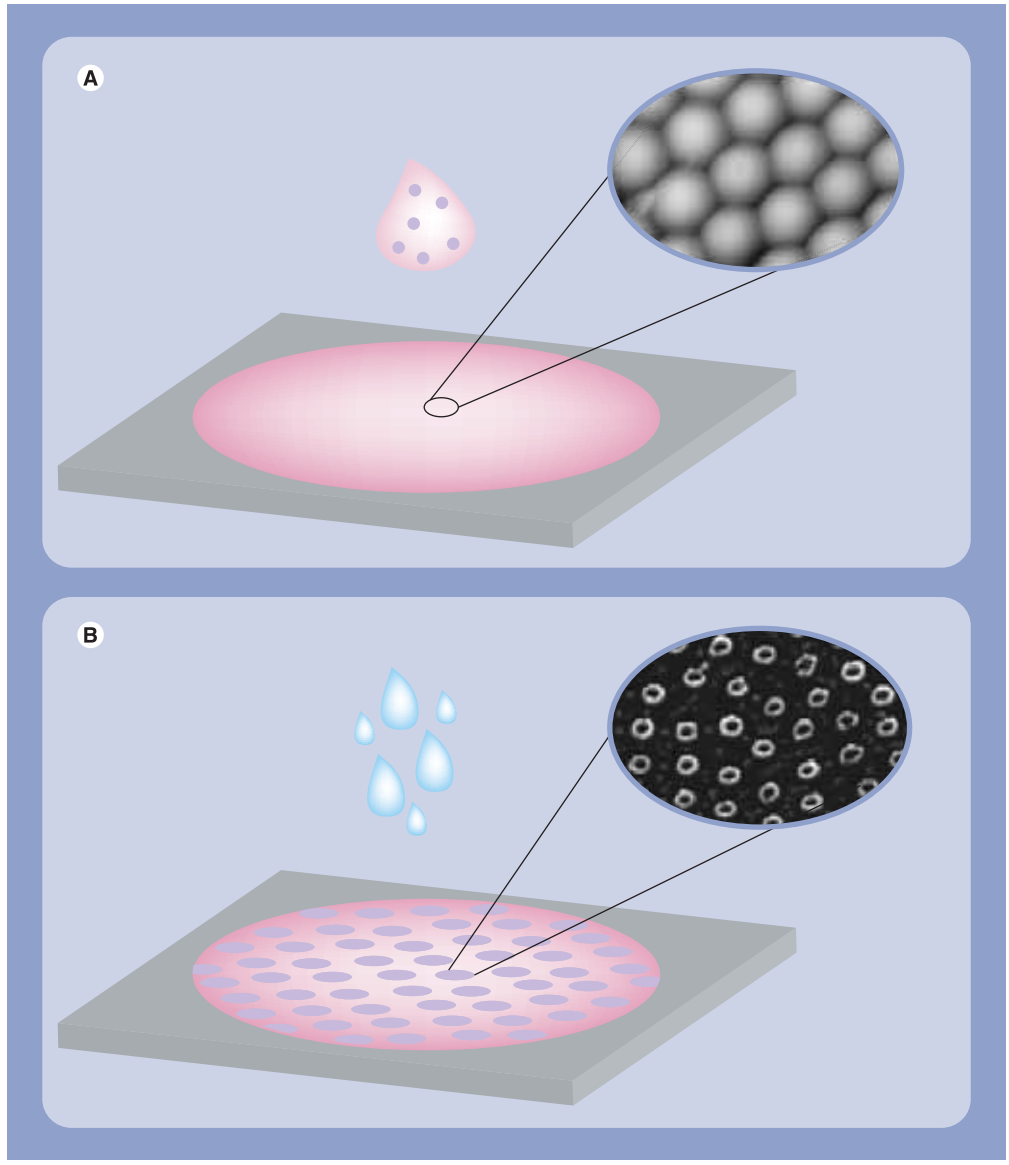

Figure 2. Example structural template formed by particle lithography with 300 nm latex mesospheres.

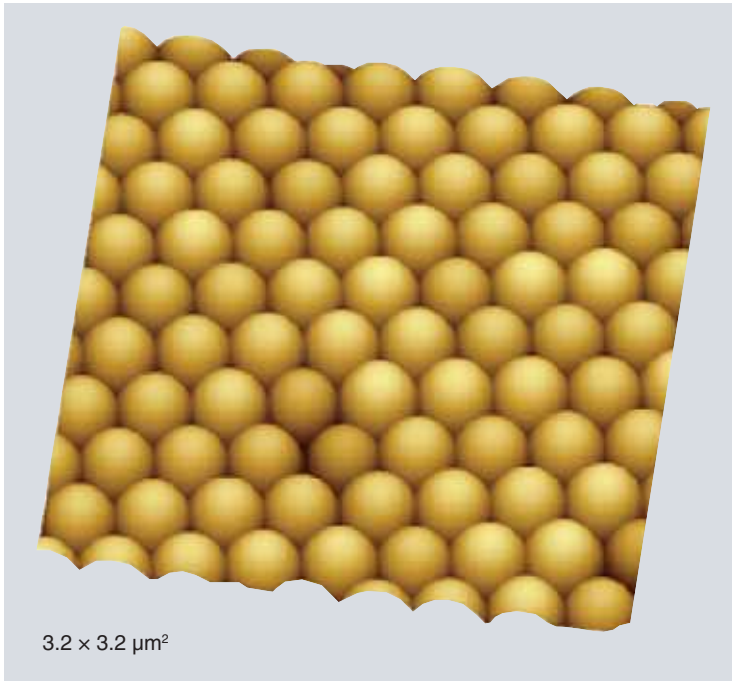

Preparation of substrates

Three different substrates were used for AFM investigations. Ruby muscovite mica was acquired from S&J Trading Inc. (Glen Oaks, NY, USA). Pieces of mica (1×1 cm^2) were cut and cleaved immediately before depositing sample solutions. Gold thin films (150 nm) evaporated on mica substrates were obtained from Agilent Technologies Inc. (Chandler, AZ, USA). A procedure reported previously for preparing ultraflat gold films on glass slides was applied to prepare template-stripped surfaces [36]. Round glass cover slides, diameter 12 mm, were obtained from Ted Pella Inc. (Redding, CA, USA). Glass slides were cleaned for 30 min by immersion in piranha solution, a 3:1 mixture of sulfuric acid and 30% hydrogen peroxide. (Caution: piranha solution is highly exothermic and corrosive.) Next, the slides were rinsed with deionized water and dried in air. For particle lithography, a volume of protein/mesosphere solution was deposited and dried on the cleaned slides.

Atomic-force microscopy

Images were acquired using an Agilent 5500 AFM/SPM system equipped with Picoscan v5.3.3 software. An ambient environment was used for AC (tapping)-mode imaging. Rectangular silicon nitride cantilevers (NSC 14/Al, resonance frequency 160 kHz, spring constant 5 N/m) from MikroMasch (Portland, OR, USA) and silicon AFM probes (Tap 150AL, resonance frequency 150 kHz, spring constant 5 N/m) with an aluminum reflex coating from Budget Sensors (Redding, CA, USA) were used for AFM imaging.

Particle lithography with proteins

Arrays of protein patterns were prepared by mixing aqueous solutions of proteins with monodisperse spheres of silica or latex at various ratios. A 10 µl drop of the mixture was deposited on a flat surface and dried at room temperature (Figure 1A). Surface coverage could be tuned to form at least one layer of spheres and varied between 1 and 4% wt/volume depending on the diameter of the particles. The monodisperse spheres form a structural template, which directs the placement of proteins on surfaces. During the drying step, mesospheres assemble spontaneously into a close-packed crystalline layer with the proteins surrounding the base of the spheres. The samples were dried under ambient humidity, which ranges from 60–64% in our air-conditioned laboratory. The final step is to remove the particles by rinsing the sample surface with deionized water (Figure 1B). The larger spheres are displaced easily by rinsing the sample; however, the proteins remain attached to the surface to form symmetric circular patterns surrounding the template spheres.

Results & discussion

For particle lithography, the natural self-assembly of monodisperse mesospheres furnish a structural template to guide and direct the placement of proteins on surfaces. Because the spheres have the same diameter, a close-packed hexagonal arrangement of latex or silica particles is produced when aqueous solutions are dried on atomically flat surfaces (Figure 2). The tightly packed mesospheres do not fully cover the surface; areas between spheres provide a conduit for aqueous protein solutions to gravitate to the surface. The model proteins chosen for our investigations are highly soluble in water. The proteins are carried with the water meniscus during ambient drying, to form regular, evenly distributed arrays of protein nanostructures at the base of the template particles. The mesospheres provide a structural template that masks spherical areas of the surface. After the templates are rinsed away, the protein nanostructures can be applied for surface investigations and assays.

Figure 3. Aggregated domains of ferritin formed naturally on mica(0001).

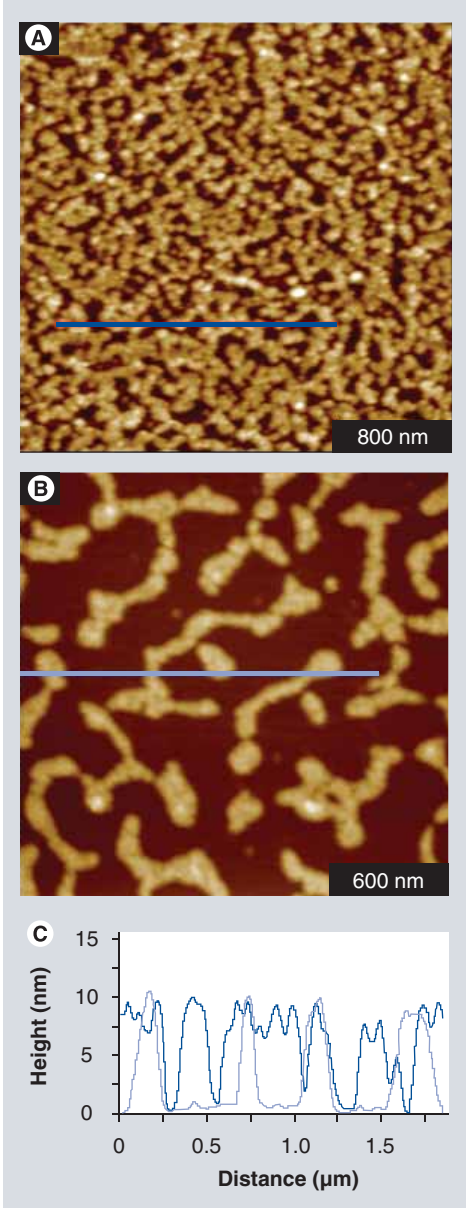

(A) High surface coverage produced with 0.5 mg/ml. **(B)** Lower coverage (0.2 mg/ml). **(C)** Combined line profiles for **A** and **B**.

Ferritin and apoferritin [37,38], BSA [39] and IgG [40] were chosen as model proteins for AFM investigations with particle lithography because of their well-studied physical and chemical properties. The direction for future investigations with the selected model proteins will be to image surface changes when binding secondary biomolecules to nanostructure arrays for fundamental analysis of protein interactions and events mediated by molecular recognition.

Films of ferritin formed by direct deposition at different concentrations

Ferritin forms the primary complex for the uptake and storage of iron in mammals. The shape of ferritin is nearly spherical and it has a diameter of 10–12 nm [41,42]. The protein structure consists of 24 subunits forming a shell containing up to 4500 iron(III) ions [37]. Ferritin is a promising component for engineering diverse nanomaterials owing to its catalytic [38,43–45], magnetic [46–48] and electrical [49,50] properties. The protein shell or cage of ferritin has been used in synthetic reactions with various metal ions to form inorganic nanoparticles of materials, such as Fe_3O_4, Co_3O_4, Mn_3O_4, CoPt, Pd, Ag, CdS and CdSe [51]. Monitoring levels of ferritin is required for the diagnosis and treatment of anemia and complications that affect iron deficiency or iron metabolism.

For AFM and surface investigations, a problem is presented for controlling the distribution and surface coverage for studies of biomolecular reactions on various substrates. Methods of sample preparation that enable control of surface coverage are useful for a range of bioanalytical applications. The process of drying, surface forces and intermolecular-attractive interactions tend to pull proteins together into tightly packed aggregates. An example is presented in Figure 3 for solutions of ferritin dried on mica under ambient conditions. Nearly monolayer coverage (84%) is achieved in Figure 3A, disclosing tightly packed assemblies of ferritin spheres. The sample was prepared by drying a 10 µl drop of an aqueous solution of ferritin (0.5 mg/ml) on a 1×1 cm^2 piece of freshly cleaved mica. The dark areas are uncovered areas of the substrate. For the examples in Figure 3, the AFM tip is unable to penetrate between proteins that are packed together closely. Thus, imaging and measurements are limited to interrogating the exposed upper surface of the clusters. By diluting samples (0.2 mg/ml), lower surface coverage (36%) is achieved; however, the proteins still tend to cluster together (Figure 3B). With an incomplete surface layer, there are only a few individual protein spheres visible between the larger domains of ferritin aggregates. A combined plot of the height of the protein layer is displayed for Figures 3A & 3B, with red- and blue-line profiles, respectively (Figure 3C). For both samples, the height measured 11 ± 2 nm, in close agreement with the known dimensions of ferritin (12 nm) obtained from x-ray crystallography [52].

Aggregation is not simply a problem for AFM surface investigations. Scaling up from the nanoscale to microarrays, the self-aggregation of protein layers affects the sensitivity and reliability of bioassays and biosensor surfaces. The sensing elements of biochips and biosensors are composed of an adsorbed layer of biomolecules or proteins for selective reaction with targeted analytes. For surface assays, detection is mediated by molecular recognition. Thus, if the target sites of immobilized proteins are inaccessible or masked by neighboring proteins, then the necessary binding reactions cannot take place. Inherently, surface-bound assays are often less sensitive than solution-based assays owing to the effects of crowding and self-aggregation.

Nanopatterns of ferritin produced on mica, gold & glass substrates

Patterns of ferritin molecules can be formed on various surfaces using particle lithography. The natural self-assembly of mesospheres provides a structural template to tune the surface coverage of proteins. Ferritin molecules can be organized into arrays of ring structures, as demonstrated for surfaces of mica, template-stripped gold and glass (Figure 4). Monodisperse spheres of colloidal silica (500 nm) were used as structural templates for the examples presented in Figure 4. For AFM topographs, the shapes of individual ferritin adsorbates can be resolved with better resolution than the previous example of Figure 3 because, at lower surface coverage, the tip can probe between molecules to profile the shape of the proteins more accurately. Topographic images are a convolution of the tip geometry and the shape of the sample. Lateral dimensions are often broader than the expected geometry for AFM topographs; however, height measurements furnish reliable information to measure the diameters of protein particles.

Successive zoom-in views of rings of ferritin on mica are viewed in Figures 4A–4C. Mica is used commonly for preparing biological samples with AFM because of the hydrophilic nature of the surface [53]. After mica is cleaved, clean and atomically flat surfaces are produced, with roughness of less than 0.1 nm. The flatness and hydrophilicity of the substrates provide an ideal platform for particle lithography. The shapes and interpattern spacing are uniform and symmetric. Because there are few defects on surfaces of mica, throughout broad areas of the surface, the AFM images reveal long-range order and periodicity. A few individual proteins are scattered in areas between the ring patterns; however, no proteins are detected inside the rings. The rings encircle bare areas of the substrate that were uncovered when the silica mesospheres were rinsed away. The displacement of template particles is complete because the spheres are removed easily by the rinsing step. The surface coverage of ferritin is approximately 17% for the sample prepared on mica. Each sample in Figure 4 was prepared at a ratio of approximately 700 ferritin per silica sphere. Approximately 6400 ferritin proteins would encapsulate a silica sphere fully; therefore, the ratio corresponds to a fraction of a monolayer shell for producing ring nanostructures. A close-up view (Figure 4B) reveals the hexagonal arrangement of the rings. A further zoom-in view of a single pattern reveals the morphology and arrangement of individual ferritin particles that form the ring (Figure 4C). The height of the rings measures 12 ± 1 nm, in close agreement with the expected diameter of ferritin. The center-to-center spacing between rings measures 550 ± 30 nm, which corresponds well to the diameter for the template silica spheres. The outer diameter of the rings for this sample measures 350 ± 20 nm (Figure 4D). To evaluate the reproducibility of the method in forming uniform pattern morphologies, additional samples were prepared 2 weeks later with 500 nm silica spheres, using the same ratios. The average width of the nanopatterns from different preparations measured 333 ± 17 nm ($n = 116$) and 319 ± 21 nm ($n = 140$), in which the reported error term is the standard deviation of the mean value. By comparing the mean values, these measurements establish that the reproducibility of particle lithography conservatively has an error term of less than 6%.

Conductive films of gold provide an electrode for electrochemistry-based measurements for biosensors and voltammetry studies. Patterns of ferritin produced on surfaces of template-stripped gold are shown with successive zoom views in Figures 4E–4G. Within the 4×4 μm^2 area of Figure 4E, there are 21 rings, in comparison to a density of 40 rings formed within the same size area of mica in Figure 4. Approximately 12% of the surface is covered with ferritin for the gold substrate. At the nanoscale, the surface of gold is rougher than mica, the roughness of the template-stripped film is approximately 0.6 nm. Thus, a few defects, such as cracks and domain boundaries, are visible on bare areas of the surface. The long-range order and periodicity of the arrays are affected by the roughness of

Figure 4. Arrays of ferritin rings produced on various surfaces using particle lithography.

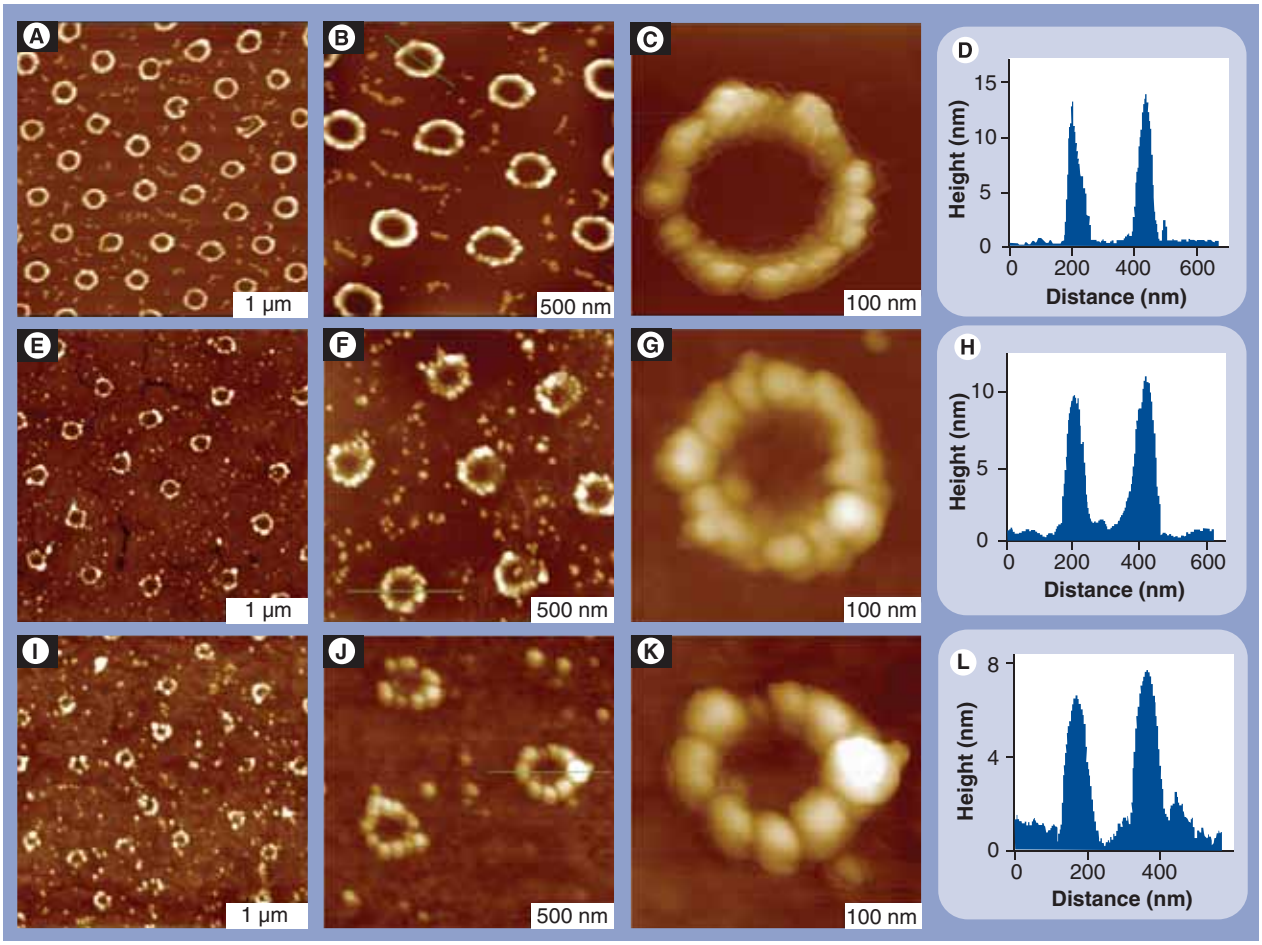

(A) Topograph (4 × 4 µm^2) for nanostructures on mica(0001). **(B)** Zoom-in view (2 × 2 µm^2). **(C)** Close-up of a single ferritin ring (0.45 × 0.45 µm^2). **(D)** Cursor profile for **B**. **(E)** Arrays of ferritin rings on template-stripped gold (3.5 × 0.5 µm^2). **(F)** Zoom-in view of **E** (1.7 × 1.7 µm^2). **(G)** A single ring pattern from **F** (0.6 × 0.6 µm^2). **(H)** Cursor profile for **F**. **(I)** Ferritin rings formed on glass (4 × 4 µm^2). **(J)** Zoom-in view of **I** (1.7 × 1.7 µm^2). **(K)** Close-up of a single ring from **J** (0.4 × 0.4 µm^2). **(L)** Line profile for **J**.

the surface, producing a few imperfections in the shapes of nanopatterns. Gold surfaces are more hydrophobic than mica, which influences the ordering and packing density of silica spheres. Fine details of the shape of the proteins within rings are revealed in zoom-in views (Figures 4F & 4G). The diameter of the rings measures 200 ± 5 nm and the height measures 11 ± 2 nm (Figure 4H). There is a significant difference between the size of the ferritin rings formed on gold and mica, which is attributed to surface wettability. The hydrophilic surface of mica results in spreading of the protein rings to span a larger area.

Nanopatterns of ferritin can also be formed on glass surfaces using particle lithography (Figures 4I–4K). Glass is an appropriate substrate for biosensing owing to the many possibilities for optical, microscopy and spectroscopy measurements. There are approximately 20 rings of ferritin within a 4 × 4 µm^2 area (Figure 4I) and approximately 19% of the surface is coated with protein. Also, the shape of the rings is not as symmetric as for mica and gold surfaces; a number of rings formed on glass are incomplete, with missing proteins. Zooming-in for a close-up view (Figure 4J), the spacing between rings measures 600 ± 30 nm, which is wider than the 500 nm diameter of the silica-mesosphere template. The periodicity is influenced by a number of parameters, such as surface treatment, roughness and hydrophobicity; however, the surface coverage and periodicity can be optimized by changing the protein:particle ratios. The results of Figure 4 demonstrate that, for different substrates, the solution conditions need to be

adjusted to optimize the density of nanostructures. By increasing the concentration of proteins, a higher surface density can be produced. A single ring structure is viewed in Figure 4K, showing the circular arrangement of proteins. The size of ferritin adsorbates is actually fairly uniform; the observed variances in height are caused by the pits and valleys of the rougher glass substrate, as well as the drying conditions of the sample. The cursor profile indicates that the rings are 7 ± 2 nm in height, which is smaller than the expected 12.5 nm dimension of ferritin (Figure 4L). The surface of glass is rougher than mica or gold, with an average roughness of 0.2–0.5 nm. The roughness profile of the glass surface is evidenced by the jagged baseline of the cursor outline (Figure 4L).

In comparing the ring structures of ferritin produced using particle lithography for various surfaces, as one can expect, there are distinct differences in the periodicity, geometry and surface coverage (Table 1). Rings of proteins prepared on the hydrophilic surface of mica have larger diameters and more proteins surrounding each ring, whereas the nanopatterns formed on gold and glass have similar periodicity but smaller ring diameters. The factors that influence the pattern morphologies are the surface roughness and wettability. During the drying step of particle lithography, the amount of spreading at the macroscopic level affects the ordering and compactness at the nanoscale.

Rings of apoferritin produced on surfaces of glass

The protein shell of ferritin without an iron core is known as apoferritin. The shell or protein cage of apoferritin consists of the same 24 subunits as ferritin, with similar dimensions. Ring structures of apoferritin molecules were produced on glass substrates using 500 nm silica spheres as a template (Figure 5). An AFM topograph (Figure 5A) displays well-organized rings of apoferritin assembled in a hexagonal arrangement, with interpattern spacing matching the diameter of the templating silica spheres. A few individual molecules of apoferritin are scattered across the surface between ring patterns and the approximate surface coverage of apoferritin is 15%. The ratio of apoferritin to silica spheres is 1000:1, approximately 15% of the number of proteins for a full layer surrounding a 500 nm sphere. In the corresponding phase image (Figure 5B), the soft and compressible areas of protein are distinct from the harder areas of the glass substrate. The morphologies of the individual proteins do not appear to be spherical; however, the shapes observed are an imaging artifact caused by the blunt, angular profile of the AFM tip. Images produced by AFM are a convolution of the shape of the imaging probe and the sample morphology. The height of the rings measures 12 ± 1 nm (Figure 5C), which is in close agreement with the known diameter of apoferritin (12 nm).

Patterns of IgG formed by particle lithography

Antibodies, such as IgG, are used for a wide range of bioassays, such as sandwich immunoassays [35,54,55]. Molecules of IgG have a Y-shaped geometry with two antibody-binding domains at the ends of a Y-like fork, which are spaced 14.5 nm apart, according to x-ray diffraction studies [56,57]. The tail of the Y-shaped molecule contains one or more carbohydrate chains. The distance between the two antibody-binding domains and the end of the carbohydrate domain is 8.5 nm. The thickness of the molecule is 4.0 nm. The hinge region at the center of the Y-shape link the amino acid chains together and is composed of disulfide bridges.

High-throughput patterning of IgG can be accomplished using particle lithography. An AFM topographic view displays 130 rings of IgG within the 10×10 μm^2 frame of Figure 6A, covering approximately 10% of the surface. At this density, approximately 130 million rings were produced for a 1×1 cm^2 sample. The ratio of IgG:spheres is 3300:1; however, because IgG has a smaller surface area than ferritin, 20,000 proteins would be needed for an

Table 1. Comparison of nanopattern morphologies on various surfaces.

Substrate	Mica	Gold	Glass
Periodicity	600 ± 30 nm	650 ± 50 nm	650 ± 70 nm
Ring diameter	360 ± 20 nm	270 ± 20 nm	290 ± 10 nm
Number of proteins per ring	15–18	10–13	9–11
Surface coverage	17%	12%	19%

Figure 5. Nanopatterns of apoferritin molecules formed on glass.

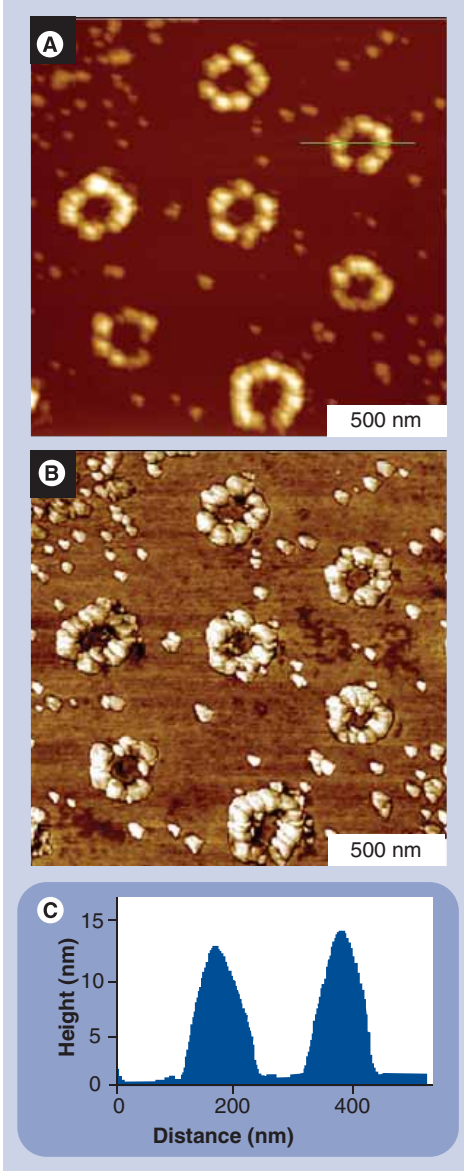

(A) Hexagonal arrangement of rings of apoferritin. **(B)** Corresponding phase image. **(C)** Cursor profile for the line in **A**.

encapsulating shell layer. In a close-up view (Figure 6B), the ring patterns exhibit a hexagonal packing arrangement, conforming to the periodicity and packing order of the structural template of 500 nm silica mesospheres. The pores of the IgG rings pinpoint the uncovered areas of the substrate where the silica mesospheres were displaced by a rinsing step. The proteins adsorb near the base of the spheres and are distributed evenly throughout the surface to form regular shapes and diameters. A 3D view reveals the uniformity of the pattern heights (Figure 6C). The corresponding 2D view (Figure 6D) and phase-contrast channel (Figure 6E) furnish details of the ring morphologies. Phase images often display surface details that cannot be resolved clearly in height images. Although the Y shape of IgG is not evident at this magnification, particles of individual proteins are apparent in the zoom views. The rings of IgG measure 5 ± 1 nm (Figure 6F) in height, which matches the dimensions for an IgG molecule that is lying flat on the surface.

Effect of protein:particle ratios

Serum albumin is the most abundant protein found in plasma and its affinity for binding materials has been well studied [58,59]. For surface bioassays, a blocking step is important to prevent nonspecific binding of proteins. Solutions of BSA are a common blocking reagent used to backfill uncovered areas of surfaces, applied in ELISA and in agglutination assays. To develop a generic approach for surface-bound protein assays, the practical step is to nanopattern BSA to prevent nonspecific binding of proteins. Therefore, BSA is a sensible choice for AFM surface investigations with nanopatterning.

When changing the ratios of proteins to mesospheres, well-defined protein nanostructures are still produced, which generate differences in surface coverage and pattern morphologies. An example in which the ratio of proteins to mesospheres was changed systematically is presented for BSA patterns formed on mica in Figure 7. At a high BSA-to-latex ratio (13,600:1), AFM topographs reveal a continuous film of BSA with an organized arrangement of circular dark holes or pores (Figures 7A–C). The areas between particles fill completely with proteins to encircle the bare cavities where the mesoparticles were displaced. A honeycomb arrangement of pores within a film of BSA is displayed in Figure 7A, produced using 300 nm latex spheres as structural templates. The periodic arrangement of dark spots is uncovered areas of mica within a monolayer film of BSA. The uncovered areas can be used to deposit a second molecule or these vacant areas can furnish an *in situ* landmark for monitoring changes in height after biochemical assays. At a high ratio, the surface coverage of BSA is 83% for Figure 7A. In comparison, approximately 22,600 BSA molecules would be required to completely surround and encapsulate a single 300 nm latex sphere. A close-up view of the surface (Figure 7B) displays the uniformity and periodicity of the patterned pores.

There are 316 pores within the 6 × 6 µm^2 area, which extrapolates to a surface density of 877 million nanostructures produced with a single 10 µl drop of protein solution placed on a 1 × 1 cm^2 area of mica. The even surface profile, symmetric patterns and regular spacing of pores is viewed clearly with a 3D representation in Figure 7C. The thickness of the protein film measures 3.8 ± 0.3 nm, matching the dimensions of a single layer of BSA (Figure 7D) and in agreement with the 4.0 nm diameter of BSA obtained by x-ray crystallography [60]. The spacing between pores measures 270 ± 20 nm, which is 10% smaller than the expected 300 nm diameter of the latex spheres. The periodicity of the resulting nanopatterns depends on the separation of latex spheres, which is observed to be 5–15% smaller than the latex diameters. Because polystyrene latex is deformable, the decrease in diameter is attributable to shrinking of latex particles when dried [9].

By using a low BSA-to-latex ratio (6800:1), ring-shaped nanopatterns of BSA were produced on mica(0001) with 300 nm latex (Figures 7E–7g). The ratio of 6800:1 corresponds to an incomplete shell of BSA encapsulating a 300 nm latex sphere, approximately half of a surrounding layer. The proteins closely surround the base of the latex to leave pore-shaped structures when the spheres are removed. The surface areas between the rings are not filled completely at this lower protein ratio (Figures 7E & 7F). A more ordered, tighter packing can be produced with changes in solution conditions. The compact hexagonal arrangement of patterns is viewed clearly in the 4 × 4 µm^2 frame, with a few BSA molecules scattered between rings. The periodicity of the nanopatterns measures 283 ± 16 nm, which matches well with the expected 300 nm diameter of the latex-templating particles. Approximately 26% of the surface is covered with rings of BSA; thus, the surface coverage can be tuned by controlling the ratio of proteins and spheres. A zoom-in topograph (1 × 1 µm^2) in Figure 7F displays a hexagonal arrangement of BSA rings. A few BSA clusters are attached to the surface between the ring-shaped nanostructures. A 3D representation of a single ring clearly reveals the assemblies of BSA molecules

Figure 6. Ring patterns of IgG produced on mica. Successive zoom-in topographs.

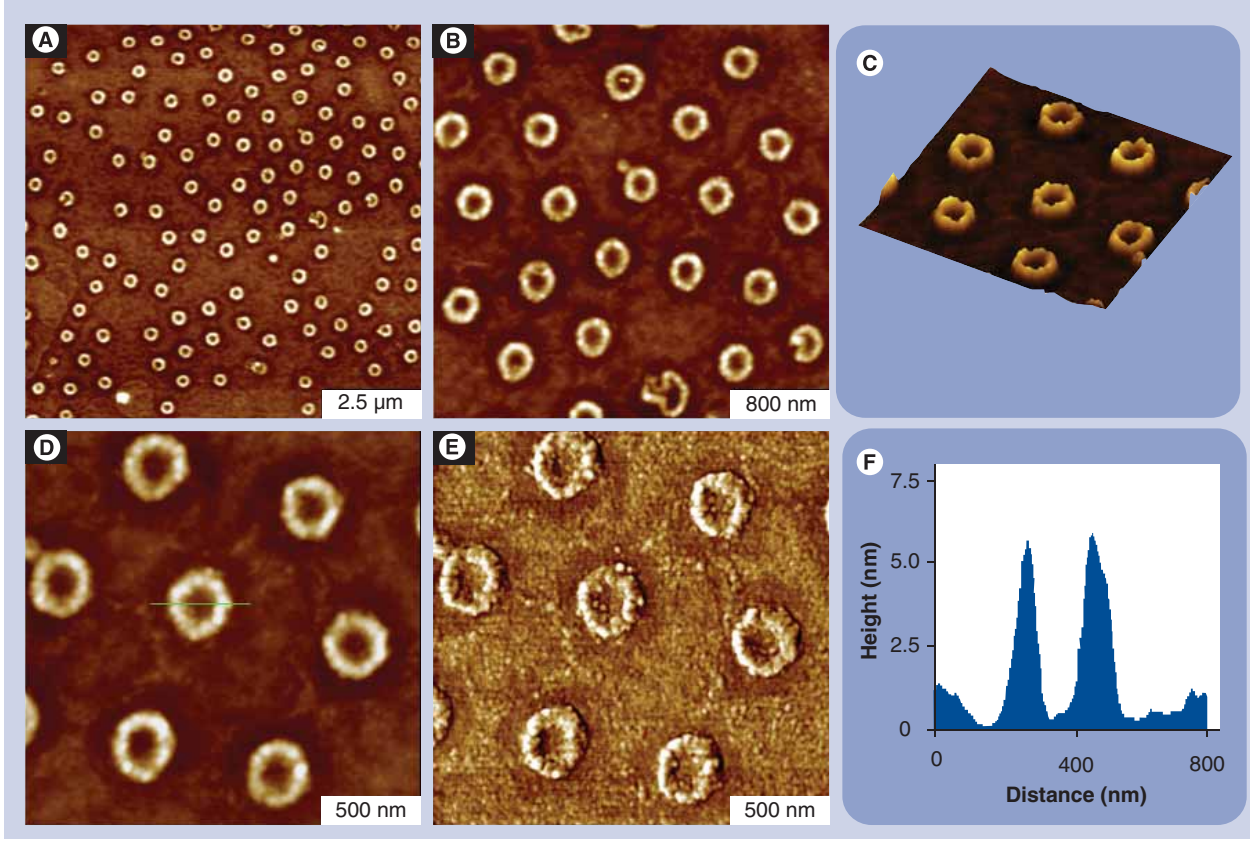

(A) 10 × 10 µm^2 ; **(B)** 3 × 3 µm^2 ; **(C)** 2 × 2 µm^2 ; **(D)** 2 × 2 µm^2 ; **(E)** phase image for **D**; **(F)** height profile for the line in **D**.

Figure 7. The ratios of protein:latex determine the morphology of patterns.

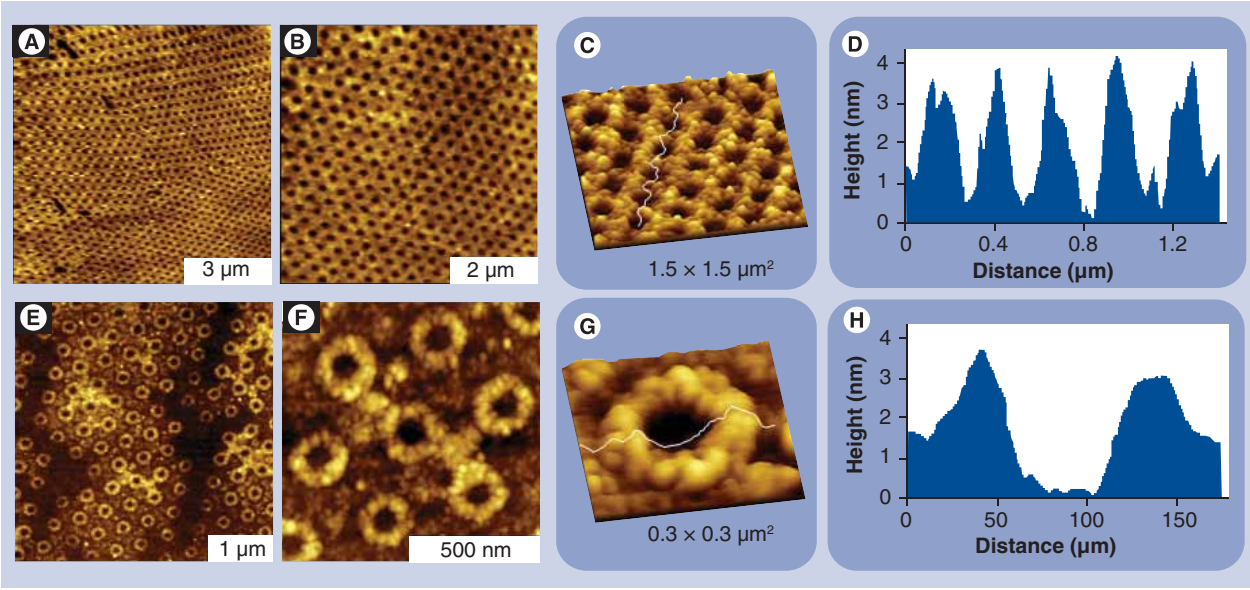

(A) AFM topograph (10 × 10 µm²) of pore-shaped structures produced at high ratio with 300 nm latex. **(B)** Zoom-in view of pore structures (6 × 6 µm²). **(C)** View of the 3D surface morphology. **(D)** Cursor profile for the line in **C**. At lower protein:latex ratio, ring-shaped structures were produced **(E)** using 300 nm spheres (4 × 4 µm²). **(F)** Zoom-in view of hexagonal arrangement of rings (1 × 1 µm²). **(G)** View of a single ring of BSA; **(H)** line profile for **G**.

(Figure 7G). The height of BSA nanostructures can be measured by referencing the uncovered areas of mica as a baseline. The height of the rings measure 3.7 ± 0.4 nm, matching the expected dimension of a single layer of BSA (Figure 7H).

Particle lithography provides a simple and effective approach for producing nanoscale protein structures. Once the experimental conditions have been chosen, dozens of samples prepared using those conditions reveal similar morphologies. The surface morphologies were highly consistent and reproducible for a given ratio and particle diameter. All of the examples of protein nanopatterns presented exhibit circular or ring-shaped nanostructures when using the solution-based approach for particle lithography. These results are different from results cited from literature reports using methods of metal evaporation, which disclose triangular or pyramid nanostructures. Our approach for solution particle lithography does not use a mask and evaporation of metals at high temperatures; rather, the mesospheres serve as a structural template during ambient drying. In solution, the proteins assemble surrounding the base of the latex or silica spheres when dried, conforming to the shape of the particle templates. Therefore, the circular ring or pore morphologies are determined by the spherical shape of the mesospheres.

Conclusion

Particle lithography is a highly reproducible approach that applies straightforward bench chemistry steps to prepare millions of individual protein nanostructures on surfaces. Particle lithography provides a high-throughput route to control the coverage and dimensions of surface structures of proteins at the scale of nms. The generality of this approach was demonstrated with various surfaces (mica, gold and glass) and different proteins (ferritin, apoferritin, IgG and BSA). By varying the ratio of proteins to mesoparticles, different pattern morphologies, such as rings or pores, are produced. The arrangement of proteins reflects the long-range order, dimensions and periodicity according to the hexagonal packing of templating mesospheres.

Future perspective

The examples presented with model proteins represent a solid beginning for the development of more complex surface-bound bioassays. Periodic arrays of nanostructures offer a valuable test platform for studies of surface chemistry at the nanoscale. A number of possible experiments and potential applications are envisioned because

well-defined arrays of nanostructures enable precise reproducible dimensions for successive measurements. As an example, for fundamental AFM investigations of reactions mediated by molecular recognition, the changes in the morphology of protein nanostructures can be monitored after chemical agents, nanoparticles or other small molecules are introduced to protein nanopatterns. Well-defined protein arrays offer precise reproducible surface features for multiple measurements. By performing experiments in aqueous buffers, studies of protein-DNA interactions and antigen–antibody binding can be accomplished by imaging the evolution of surface changes during biochemical reactions. The particle templates used for preparing test platforms can be scaled to ever smaller dimensions, for studies of size-dependent properties at tens of nanometers, approaching single-molecule detection.

Financial & competing interests disclosure

The authors gratefully acknowledge financial support from the Louisiana Board of Regents, Research Competitiveness Subprogram, (LEQSF(2006–09)-RD-A-04), the American Chemical Society Petroleum Research Foundation (G43352-G5) and the LSU Council on Research Faculty Seed Grant. Jie-Ren Li thanks Pfizer Corporation for a graduate fellowship in analytical chemistry and Stephanie Daniels was supported by the NSF-LAMP program.

The authors have no other relevant affiliations or financial involvement with any organization or entity with a financial interest in or financial conflict with the subject matter or materials discussed in the manuscript apart from those disclosed.

No writing assistance was utilized in the production of this manuscript.

Ethical conduct of research

The authors state that they have obtained appropriate institutional review board approval or have followed the principles outlined in the Declaration of Helsinki for all human or animal experimental investigations. In addition, for investigations involving human subjects, informed consent has been obtained from the participants involved.

Executive summary

- There is a growing need for methods that can create organized arrays of nanomaterials reproducibly with high throughput and low-cost. Particle lithography provides such an approach for rapidly preparing millions of exquisitely uniform nanometer-sized structures on flat surfaces using basic steps of benchtop chemistry.
- Surface self-assembly is emerging as an indispensable approach for organizing materials at the molecular scale for practical reasons, such as low cost, applicability to a wide range of nanomaterials and capabilities for high-throughput manufacture of regularly shaped surface structures.
- Unlike methods of particle lithography with metal evaporation, which produce periodic arrays of triangular structures, solution-based particle lithography creates rings and pore-shaped geometries.
- Particle lithography provides a toolkit for fabricating protein nanopatterns on flat surfaces, providing superb control of the spacing and arrangement of nanostructures. With particle lithography, chemists can inexpensively produce robust, regular nanostructures using the conventional tools of mixing, centrifuging and drying.

ve summary

article lithography, millions of nanostructures can be prepared on a range of different surfaces with relatively few defects gh reproducibility. The nanopatterns may potentially be applied for engineering the surfaces of biochips and biosensors.

Bibliography

1. Blattler T, Huwiler C, Ochsner M *et al.*: Nanopatterns with biological functions. *J. Nanosci. Technol.* 6(8), 2237–2264 (2006).
2. Yonson CR, Stuart DA, Zhang X, McFarland AD, Haynes CL, VanDuyne RP: Towards advanced chemical and biological nanosensors – an overview. *Talanta* 67, 438–448 (2005).
3. Choi DG, Jang SG, Yu HK, Yang SM: Two-dimensional polymer nanopattern by using particle-assisted soft lithography. *Chem. Mater.* 16(18), 3410–3413 (2004).
4. Han SB, Briseno AL, Shi XY, Mah DA, Zhou FM: Polyelectrolyte-coated nanosphere lithographic patterning of surfaces: fabrication and characterization of electropolymerized thin polyaniline honeycomb films. *J. Phys. Chem. B* 106(25), 6465–6472 (2002).
5. Yi DK, Kim D-Y: Polymer nanosphere lithography: fabrication of an ordered trigonal polymeric nanostructure. *Chem. Commun. (Camb.)* 982–983 (2003).
6. Sun Z, Li Y, Wang Y *et al.*: Three-dimensional colloidal crystal-assisted lithography for two-dimensional patterned arrays. *Langmuir* 23, 10725–10731 (2007).

7. Cai Y, Ocko BM: Large-scale fabrication of protein nanoarrays based on nanosphere lithography. *Langmuir* 21(20), 9274–9279 (2005).
8. Valsesia A, Meziani T, Bretagnol F, Colpo P, Ceccone G, Rossi F: Plasma assisted production of chemical nano-patterns by nano-sphere lithography: application to bio-interfaces. *J. Phys. D Appl. Phys.* 40, 2341–2347 (2007).
9. Garno JC, Amro NA, Wadu-Mesthrige K, Liu G-Y: Production of periodic arrays of protein nanostructures using particle lithography. *Langmuir* 18(21), 8186–8192 (2002).
10. Li J-R, Henry GC, Garno JC: Fabrication of nanopatterned films of bovine serum albumin and staphylococcal protein A using latex particle lithography. *Analyst* 131(2), 244–250 (2006).
11. Hulteen JC, Treichel DA, Smith MT, Duval ML, Jensen TR, Van Duyne RP: Nanosphere lithography: Size-tunable silver nanoparticle and surface cluster arrays. *J. Phys. Chem. B* 103(19), 3854–3863 (1999).
12. Bullen HA, Garrett SJ: TiO_2 nanoparticle arrays prepared using a nanosphere lithography technique. *Nano Lett.* 2(7), 739–745 (2002).
13. Cheng SL, Lu SW, Wong SL, Chang CC, Chen H: Fabrication of 2D ordered arrays of cobalt silicide nanodots on (001)Si substrates. *J. Cryst. Growth* 300, 473–477 (2007).
14. Zhang G, Wang D, Mohwald H: Ordered binary arrays of Au nanoparticles derived from colloidal lithography. *Nano Lett.* 7(1), 127–132 (2007).
15. Liu DF, Xiang YJ, Liao Q *et al.*: A simple route to scalable fabrication of perfectly ordered ZnO nanorod arrays. *Nanotechnology* 18, 1–5 (2007).
16. Zin MT, Leong K, Wong N-Y, Ma H, Jen AK-Y: Plasmon resonant structures with unique topographic characteristics and tunable optical properties for surface-enhanced Raman scattering. *Nanotechnology* 8, 1–6 (2007).
17. Li Y, Li C, Cho SO, Duan G, Cai W: Silver hierarchical bowl-like array: synthesis, superhydrophobicity, and optical properties. *Langmuir* 23, 9802–9807 (2007).
18. Weekes SM, Ogrin FY, Murray WA, Keatley PS: Macroscopic arrays of magnetic nanostructures from self-assembled nanosphere templates. *Langmuir* 23, 1057–1060 (2007).
19. Ctistis G, Patoka P, Wang X, Kempa K, Giersig M: Optical transmission through hexagonal arrays of subwavelength holes in thin metal films. *Nano Lett.* 7(9), 2926–2930 (2007).
20. Wang XD, Summers CJ, Wang ZL: Large-scale hexagonal-patterned growth of aligned ZnO nanorods for nano-optoelectronics and nanosensor arrays. *Nano Lett.* 4(3), 423–426 (2004).
21. Wu W, Katsnelson A, Memis OG, Mohseni H: A deep sub-wavelength process for the formation of highly uniform arrays of nanoholes and nanopillars. *Nanotechnology* 8, 1–4 (2007).
22. Ryu KM, Badmaev A, Gomez L, Ishikawa F, Lei B, Zhou CW: Synthesis of aligned single-walled nanotubes using catalysts defined by nanosphere lithography. *J. Am. Chem. Soc.* 129(33), 10104–10105 (2007).
23. Wang Y, Han SB, Briseno AL, Sanedrin RJG, Zhou FM: A modified nanosphere lithography for the fabrication of aminosilane/polystyrene nanoring arrays and the subsequent attachment of gold or DNA-capped gold nanoparticles. *J. Mater. Chem.* 14(24), 3488–3494 (2004).
24. McLellan JM, Geissler M, Xia YN: Edge spreading lithography and its application to the fabrication of mesoscopic gold and silver rings. *J. Am. Chem. Soc.* 126(35), 10830–10831 (2004).
25. Geissler M, McLellan JM, Chen JY, Xia YN: Side-by-side patterning of multiple alkanethiolate monolayers on gold by edge-spreading lithography. *Angew. Chem. Int. Ed. Engl.* 44(23), 3596–3600 (2005).
26. Nakamura H, Karube I: Current research activity in biosensors. *Anal. Bioanal. Chem.* 377, 446–468 (2003).
27. Agheli H, Malmstrom J, Larsson EM, Textor M, Sutherland DS: Large area protein nanopatterning for biological applications. *Nano Lett.* 6(6), 1165–1171 (2006).
28. Lueking A, Horn M, Eickhoff H, Bussow K, Lehrach H, Walter G: Protein microarrays for gene expression and antibody screening. *Anal. Biochem.* 270(1), 103–111 (1999).
29. Saviranta P, Okon R, Brinker A, Warashina M, Eppinger J, Geierstager B: Evaluating sandwich immunoassays in microarray format in terms of the ambient analyte regime. *Clin. Chem.* 50(10), 1907–1920 (2004).
30. Zhu H, Bilgin M, Bangham R *et al.*: Global analysis of protein activities using proteome chips. *Science* 293(5537), 2101–2105 (2001).
31. Robinson WH, DiGennaro C, Hueber W *et al.*: Autoantigen microarrays for multiplex characterization of autoantibody responses. *Nat. Med.* 8(3), 295–301 (2001).
32. Huff JL, Lynch MP, Nettikadan S, Johnson JC, Vengasandra S, Henderson E: Label-free protein and pathogen detection using the atomic force microscope. *J. Biomol. Screen.* 9(6), 491–497 (2004).
33. Allen S, Chen X, Davies J *et al.*: Detection of antigen–antibody binding events with the atomic force microscope. *Biochemistry* 36, 7457–7463 (1997).
34. Lee K-B, Kim E-Y, Mirkin CA, Wolinsky SM: The use of nanoarrays for highly sensitive and selective detection of human immunodeficiency virus type 1 in plasma. *Nano Lett.* 4(10), 1869–1872 (2004).
35. Haab BB: Applications of antibody array platforms. *Curr. Opin. Biotechnol.* 17, 415–421 (2006).
36. Hegner M, Wagner P, Semenza G: Ultralarge atomically flat template-stripped Au surfaces for scanning probe microscopy. *Surf. Sci.* 291(1–2), 39–46 (1993).
37. Cowley JM, Janney DE, Gerkin RC, Buseck PR: The structure of ferritin cores determined by electron nanodiffraction. *J. Struct. Biol.* 131(3), 210–216 (2000).
38. Theil EC, Matzapetakis M, Liu X: Ferritins: iron/oxygen biominerals in protein nanocages. *J. Biol. Inorg. Chem.* 11, 803–810 (2006).
39. Peters T, Feldhoff RC: Fragments of bovine serum-albumin produced by limited proteolysis – isolation and characterization of tryptic fragments. *Biochemistry* 14(15), 3384–3391 (1975).
40. Saphire EO, Parren P, Pantophlet R *et al.*: Crystal structure of a neutralizing human IgG against HIV-1: a template for vaccine design. *Science* 293(5532), 1155–1159 (2001).
41. Pereira AS, Small W, Krebs C *et al.*: Direct spectroscopic and kinetic evidence for the involvement of a peroxodiferric intermediate during the ferroxidase reaction in fast ferritin mineralization. *Biochemistry* 37(28), 9871–9876 (1998).
42. Harrison PM, Theil EC: The ferritins: molecular properties, iron storage function and cellular regulation. *Biochim. Biophys. Acta* 1275(3), 161–203 (1996).
43. Roginsky VA, Barsukova TK, Bruchelt G, Stegmann HB: Iron bound to ferritin catalyzes ascorbate oxidation: effects of

chelating agents. *Biochim. Biophys. Acta* 1335, 33–39 (1997).

44. Dechakiatkrai C, Chen C, Lynam C *et al.*: Direct ascorbic acid detection with ferritin immobilized on single-walled carbon nanotubes. *Electrochem. Solid St.* 11(1), K4–K6 (2008).
45. Yu Q, Qin G, Li H, Xia Z, Nian Y, Pei S-S: Mechanism of horizontally aligned growth of single-wall carbon nanotubes on R-plane sapphire. *J. Phys. Chem. B* 110, 22676–22680 (2006).
46. Lopez A, Gutierrez L, Lazaro FJ: The role of dipolar interaction in the quantitative determination of particulate magnetic carriers in biological tissues. *Phys. Med. Biol.* 52, 5043–5056 (2007).
47. Guertin RP, Harrison N, Zhou ZX, McCall S, Drymiotis F: Very high field magnetization and AC susceptibility of native horse spleen ferritin. *J. Magn. Magn. Mater.* 308, 97–100 (2007).
48. Clemente-Leon M, Coronado E, Soriano-Portillo A *et al.*: Magnetic Langmuir-Blodgett films of ferritin with different iron contents. *Langmuir* 22, 6993–7000 (2006).
49. Xu DG, Watt GD, Harb JN, Davis RC: Electrical conductivity of ferritin proteins by conductive AFM. *Nano Lett.* 5(4), 571–577 (2005).
50. Liu G, Debnath S, Paul KW *et al.*: Characterization and surface reactivity of ferrihydrite nanoparticles assembled in ferritin. *Langmuir* 22, 9313–9321 (2006).
51. Klem MT, Resnick DA, Gilmore K, Young M, Idzerda YU, Douglas T: Synthetic control over magnetic moment and exchange bias in all-oxide materials encapsulated within a spherical protein cage. *J. Am. Chem. Soc.* 129(1), 197–201 (2007).
52. Takagi H, Shi DS, Ha Y, Allewell NM, Theil EC: Localized unfolding at the junction of three ferritin subunits – a mechanism for iron release? *J. Biol. Chem.* 273(301), 18685–18688 (1998).
53. Muller DJ, Amrein M, Engel A: Adsorption of biological molecules to a solid support for scanning probe microscopy. *J. Struct. Biol.* 119, 172–188 (1997).
54. Nielsen UB, Geierstanger BH: Multiplexed sandwich assays in microarray format. *J. Immunol. Methods* 290, 107–120 (2004).
55. Lynch M, Mosher C, Huff J, Nettikadan S, Johnson J, Henderson E: Functional protein nanoarrays for biomarker profiling. *Proteomics* 4(6), 1695–1702 (2004).
56. Silverton EW, Navia MA, Davies DR: 3-Dimensional structure of an intact

human immunoglobulin. *Proc. Natl Acad. Sci. USA* 74(11), 5140–5144 (1977).

57. Sarma VR, Silverto EW, Davies DR, Terry WD: 3-Dimensional structure at 6 A resolution of a human γ GL immunoglobulin molecule. *J. Biol. Chem.* 246(11), 3753–3759 (1971).
58. Sugio S, Kashima A, Mochizuki S, Noda M, Kobayashi K: Crystal structure of human serum albumin at 2.5 angstrom resolution. *Protein Eng.* 12(6), 439–446 (1999).
59. Peters T: *All about albumin.* Academic Press, San Diego, USA (1996).
60. Rosenoer VM, Oratz M, Rothschilde MA: *Albumin Structure and Function.* Pergamon Press, NY, USA (1977).